Journal of Additive Manufacturing Technologies
DOI: 10.18416/JAMTECH. 24121160

Infinite Science | Publishing

Functional island scanning strategy for powder bed fusion

Ö. S. Çavuş[1,2,3], S. Khalilvandi Behrouzyar[1,2,3], and B. Koç[1,2,3*]

[1] *Faculty of Engineering and Natural Sciences, Sabanci University, Istanbul 34956 ,Turkey*
[2] *Integrated Manufacturing Technologies Research and Application Center, Sabanci University, Istanbul 34906, Turkey*
[3] *Composite Technologies Center of Excellence, Istanbul Technology Development Zone, Sabanci University-Kordsa Global, Istanbul 34956, Turkey*
[*] *Corresponding author, email: bahattin.koc@sabanciuniv.edu*

Abstract

Energy is transferred from the energy beam to the processed material during Powder Bed Fusion (PBF) process. The high energy input and uneven temperature distribution can result in a substantial temperature gradient, leading to significant thermal stress and warping deformation. One of the most influential factors in the material processing of additive manufacturing is the choice of scanning strategies. Therefore, optimizing the scanning strategy can help achieving a more even heat distribution across the part and reduce thermal distortion, which is crucial for producing high-quality L-PBF components. In this study, we developed a modified island scanning strategy and thermal management approach which is related ordering the scanning sequence of islands, similar to Traveling Salesman Problem (TSP) variant and it is also adapted for multiple laser cases. The introduction of modified island scan strategies aims to preserve the geometric integrity of the part, minimize distortion, and optimize the scanning process by considering the part's geometric features, all while achieving the desired mechanical properties. The results demonstrate that solving the TSP with a genetic algorithm (GA) is suitable for both single and multi-laser systems. Additionally, the functional island scanning strategy is effective for optimizing the lengths of scanning vectors. Furthermore, the island scanning strategy proves to be superior to the raster strategy in terms of thermal uniformity.

Keywords: Selective laser melting, Island scanning strategy, Finite element analysis

1. Introduction

Additive manufacturing (AM) builds complex objects layer by layer from a CAD model, offering an efficient way to produce shapes difficult to produce with traditional methods. It excels in creating intricate geometries. In metal AM, the main techniques are Directed Energy Deposition (DED) and Powder Bed Fusion (PBF), with PBF subdivided into Electron Beam Melting (EBM), Selective Laser Melting (SLM), Selective Laser Sintering (SLS), and Direct Metal Laser Sintering (DMLS). The fundamental difference is that melting fully liquefies the powder, while sintering bonds particles below their melting point [1].

Numerous methodologies have been explored in the literature concerning the impact of scanning strategy variables on the quality of manufactured parts. Essentially, long scan vectors have been observed to induce greater heat accumulation compared to their shorter counterparts. Consequently, this heightened heat accumulation ultimately results in increased residual stress and diminished overall part quality [2], [3], [4]. Considering the hatch patterns, one of the standard strategies to decrease residual stress is to prefer the checkerboard pattern. As a result of the reduction of residual stresses, mechanical properties have improved [2], [5], [6]. In addition, Parry et al. [7] reached noteworthy results regarding scan length, geometry, and the geometry of the scanned area, indicating that the geometry of the scan vector can cause localized heat accumulation and suggesting that minimizing scan vector length variance and avoiding scan vectors longer than 2.5 mm are crucial. In their research, Cheng et al. [8] conducted a simulation to test using islands in the scan paths and changing their direction for each layer, essentially rotating the scan direction layer by layer. Their findings revealed that this method could lead to the production of parts with more evenly distributed residual stresses, indicating a potential improvement in the quality and durability of the manufactured parts. Furthermore, they demonstrated that the island scanning strategy reduced the maximum peak temperature due to the short scanning path. Masoomi et al. [9] indicated that island scanning, by enabling shorter track lengths, effectively decreases the magnitude of residual stress.

Zou et al. [10], stated that scan sequence is another variable to decrease residual stress, especially for the multi-laser case. In their work, Ramos et al. [11] proposed a scanning sequence for island scanning strategy that ensures the following scan island is not neighboring the two previous islands to disperse the heat across the part.

Significantly, the scanning strategy, which refers to the specific geometric route taken by the energy beam, has a distinct impact on thermal gradients, residual stress,

and imperfections. Consequently, the subject of scanning strategy receives extensive attention in scholarly research, approached from various perspectives. Ongoing endeavors are directed towards refining this strategy to enhance the overall quality of the manufactured components. Numerical simulation serves as a powerful tool for forecasting thermal behavior, residual stress, and deformation in parts prior to production, guaranteeing favorable results with a satisfactory level of precision. Finite element analysis (FEA) stands out as one of the premier numerical techniques for examining the complex, multi-physical aspects of PBF [12], [13], [14].

Furthermore, Multiple PBF represents a significant advancement in the field of AM, offering the potential to substantially increase production efficiency [15], [16]. Nevertheless, there is a need to enhance research efforts in this domain.

On the other hand, it is controversial to what extent these strategies consider the geometric properties of the part to be produced. Island strategies are prominent in dissipating heat and reducing residual stress, avoiding very long scan vectors. However, island geometry is usually square and cannot accurately represent the geometry to be produced. In this study, a modified island scanning strategy, and heat management algorithm have been proposed. Moreover, the issue of determining the optimal scanning sequence for the islands was addressed by Traveling Salesman Problem (TSP), which was then efficiently solved using a genetic algorithm (GA). In the case of multiple lasers, the problem can be viewed as a Multiple TSP (MTSP). The next sections cover the generation of island scanning strategy procedure, scan sequencing scheme for both single and multiple laser cases and thermal analysis results. Finally, future work and challenges are discussed.

2. Material and methods

2.1. Formulations for scanning strategy development

Scanning strategies are built upon geometric definitions and formulas. This section summarizes key concepts, focusing on parametric forms for clarity and practical application.

A planar curve is defined by $\vec{r}(t)=[x(t),y(t)]$, mapping an interval [a, b] onto $\mathbb{R}^2$. Here, x(t) and y(t) are coordinate functions. For three-dimensional curves, the representation is $\vec{r}(t)=[x(t),y(t),z(t)]$.

A surface is parametrized by $\vec{r}(u,v)=[x(u,v),y(u,v),z(u,v)]$, with x(u, v), y(u, v), and z(u, v) as functions of u, and v.

B-rep models define a 3D object by its surfaces, composed of faces, edges, and vertices, which correspond to surfaces, curves, and points, respectively. Intersection refers to coincidence elements at the junction of multiple geometric entities, including point-point, point-curve, point-surface, curve-curve, curve-surface, and surface-surface intersections.

Two points $\mathbf{r}_1$ and $\mathbf{r}_2$ intersect if:

$$\| \mathbf{r}_1 - \mathbf{r}_2 \| < \varepsilon \tag{1}$$

A point $\mathbf{r}_0$ intersects with a parametric curve $\mathbf{r}(t)$, $0 \le t \le 1$, by minimizing:

$$F(t) = \| \mathbf{r}(t) - \mathbf{r}_0 \|^2 \tag{2}$$

For a point $\mathbf{r_0}$ and an implicit surface $f(\mathbf{r})=0$, the intersection condition is:

$$|f(\mathbf{r}_0)| < \varepsilon, \quad \frac{|f(\mathbf{r}_0)|}{\| \nabla f(\mathbf{r}_0) \|} < \delta \tag{3}$$

Parametric curves $\mathbf{r}_1(t)$ and $\mathbf{r}_2(\sigma)$, $0 \le t, \sigma \le 1$ intersect by minimizing:

$$D(t,\sigma) = \| \mathbf{r}_1(t) - \mathbf{r}_2(\sigma) \|^2 \tag{4}$$

A parametric curve $\mathbf{r}_1(t)$ intersects a parametric surface $\mathbf{r}_2(u,v)$, $0 \le t,u,v \le 1$, by minimizing:

$$F(t,u,v) = \| \mathbf{r}_1(t) - \mathbf{r}_2(u,v) \|^2 \tag{5}$$

This overview outlines the mathematical foundations essential for developing and analyzing scanning strategies.

2.2. Mathematical model for transient thermal simulation

Predicting the development of thermal fields in IN 718 L-PBF involves the creation of computer simulation models based on 3D FEM modelling. These models address transient heat transfer challenges intrinsic to the L-PBF process by utilizing a 3D heat convection equation.

$$\rho c \dot{T} = \dot{Q} + \nabla.(k \nabla T) - h(T - T_{amb}) - \epsilon \sigma (T^4 - T_{amb}^4) \tag{6}$$

Where ρ is mass density, c is the specific heat, T is temperature, t is time, $\dot{Q}$ is the rate of internal heat generation per unit volume, k is thermal conductivity, h is convection coefficient, ϵ is emissivity, σ is the Stefan-Boltzmann constant, and T_{amb} is ambient temperature.

The discretized temperature field and its gradients for the thermal FEA problem are shown below:

$$[\mathrm{C}][\dot{\mathrm{T}}] + ([\mathrm{K}]+[\mathrm{H}]) = \mathrm{R}_T \tag{7}$$

In the equation, $[C]$,$[K]$, and $[H]$ are specific energy storage, conduction, and convection stiffness matrices

and R_T is the total vectors of force (heat flux, convection, radiation, heat generation).

The volumetric Gaussian heat source was used to represent the laser heat input. The heat source model was proposed by Goldak et al. [17].

$$Q = \frac{6\sqrt{3}P\mu}{\pi\sqrt{\pi}r_x r_y r_z} exp\left[-\frac{3x^2}{r_x^2} - \frac{3y^2}{r_y^2} - \frac{3z^2}{r_z^2}\right] \quad (8)$$

Where P is laser power, μ is lumped efficiency term, r_x, r_y radius of the laser beam, r_z penetration depth and $x, y,$ and z the distances between integration points and heat source.

Accounting for the heat losses represented in the equations, essential to consider heat dissipation due to evaporation. When subjected to high laser irradiation, the surface temperature of a molten pool can surpass the substance's boiling point. Consequently, this drives the formation of metal vapour on the pool's surface, which subsequently separates, carrying a substantial amount of thermal energy away. Accordingly, one calculates the evaporation loss as shown:

$$q_{evap} = \frac{0.82\Delta H_v}{\sqrt{2\pi MRT_s}} P_0 exp\left(\frac{\Delta H_v (T_s - T_v)}{RT_s T_v}\right) \quad (9)$$

In this equation, ΔH_v is the effective enthalpy of metal vapour, M is the molar mass of metal vapour, T_s is the temperature of the surface, T_v is boiling temperature, and P_0 is atmospheric pressure. The material properties for IN 718 are provided in Table 1.

Table 1. Material Properties of IN718 alloy [18]

Material Properties	Values	Nomenclature
Solidus Temperature [K]	1528	T_s
Liquidus Temperature [K]	1610	T_l
Gas conductivity [W/m/k]	0.016	D_p
Average powder particle size [m]	3×10^{-5}	k
Powder volume fraction	0.3	ϕ
Evaporation enthalpy [J/kg]	6.4×10^{-6}	ΔH_v
Molar mass [kg/mol]	5.975×10^{-2}	M

A state variable was employed to monitor the condition of individual elements by utilizing a discrete variable with three distinct criteria, facilitating the assignment of appropriate material characteristics.

$$f(x) = \begin{cases} -1, & \text{if } powder \\ 0, & \text{if } liquid \\ +1, & \text{if } solid \end{cases} \quad (10)$$

MSC Marc is a comprehensive FEA software widely recognized for its capabilities in nonlinear simulations. It can perform a range of simulations, including thermal, structural, and multi-physics. The software allows for the definition of specific material behaviors, loading conditions, and boundary constraints through user-defined subroutines, which can be developed in the FORTRAN language. This makes it particularly well-suited for complex, nonlinear simulations such as AM process simulations. In this study, several user subroutines, such as UACTIVE, FLUX, UTIMESTEP, ANKOND and USPCHT were incorporated into the model. After coding the user subroutines with Visual Studio 2022 [19], MSC Marc 2023.04 [20] was used as the FEM solver to run the thermal simulations. Iso-parametric 8-node hexahedral elements are utilized in the current simulations. Due to the small size of the heat source in the L-PBF process (approximately 50 μm), precise domain discretization is essential to capture its movement and accurately predict the temperature evolution during AM Process. Selecting very fine mesh sizes increases computational expense in terms of simulation time. Therefore, mesh sizes of 20 μm were chosen based on various mesh dependency analyses. Additionally, a mesh coarsening scheme was implemented for the base plate meshes. A schematic view of the FE model, meshes, elements and boundary conditions used in the simulations in Fig. 1.

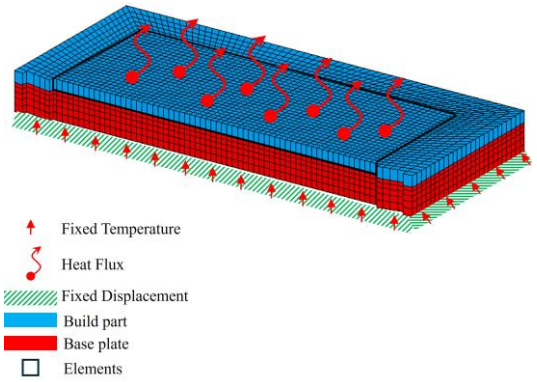

Fig. 1 Finite element model, meshes, elements and boundary conditions

2.3. Theoretical basis for GA

GAs are a class of evolutionary algorithms that mimic the process of natural selection to solve optimization and search problems. The mathematical framework of GAs involves several key components:

- Representation (Chromosomes)
- Fitness Function

- Selection
- Crossover (Recombination)
- Mutation

In GAs, potential solutions to an optimization problem are encoded as chromosomes. A chromosome is typically represented as a string of characters, which could be binary, real numbers, or any discrete set:

$$C = (g_1, g_2, \ldots, g_n) \tag{11}$$

where C is a chromosome consisting of genes $g_1, g_2, \ldots, g_n$.

The fitness function, $f(C)$, evaluates how well a chromosome C solves the optimization problem. The goal of the GA is to maximize (or minimize) this fitness function:

$$\text{Maximize } f(C) \quad \text{or} \quad \text{Minimize } f(C) \tag{12}$$

Selection is the process by which chromosomes are chosen from the population to create offspring for the next generation. The probability of selection is often proportional to the fitness of the chromosomes:

$$P(C_i) = \frac{f(C_i)}{\sum_{j=1}^{N} f(C_j)} \tag{13}$$

where $P(C_i)$ is the selection probability of chromosome C_i, and N is the total number of chromosomes in the population.

Crossover, or recombination, is a genetic operator used to combine the genetic information of two parents to generate new offspring:

$$C_{\text{offspring}} = \text{crossover}(C_{\text{parent1}}, C_{\text{parent2}}) \tag{14}$$

Mutation introduces random changes to the offspring chromosomes to maintain genetic diversity within the population:

$$C_{\text{mutated}} = \text{mutation}(C_{\text{offspring}}) \tag{15}$$

The GA iterates through the following steps until a termination condition is met:

1. Initialize the population of chromosomes.
2. Evaluate the fitness of each chromosome in the population.
3. Select parents from the current population.
4. Perform crossover and mutation to generate new offspring.
5. Form the next generation.
6. Repeat steps 2-5.

3. Results and discussion

3.1. Verification of thermal model

The thermal model's validation is achieved through numerical finite element results derived from the study conducted by Chen et al. [21]. Their research employed an FEM model to simulate the Laser Powder Bed Fusion (L-PBF) process, with findings corroborated by experimental data. The simulation was carried out on a domain of $600 \times 300 \times 120 \mu m^3$, utilizing Goldak's double ellipsoid point heat source model. Default settings were applied, which included a power of $285W$, a laser scan speed of 960mm/s, and preheating the building platform to 80°C. Additionally, the rotation of hatch lines across successive layers was set at 67°, the hatch distance (h_d) was $110\mu m$, and the dwell time (r_t) was 10 seconds. Our study focuses solely on single-layer analyses, and comparisons for the first layer reveal that the difference between the two results is approximately 3%. This indicates that our model is in good agreement with the work of [21]. Table 2 and Fig. 2 illustrates the results.

Table 2. Comparison of temperature data

Layer	Power (W)	Speed (mm/s)	Temperatures (K)	Chen (K)	Diff. (%)
1	285	960	3578	3680	-3.0

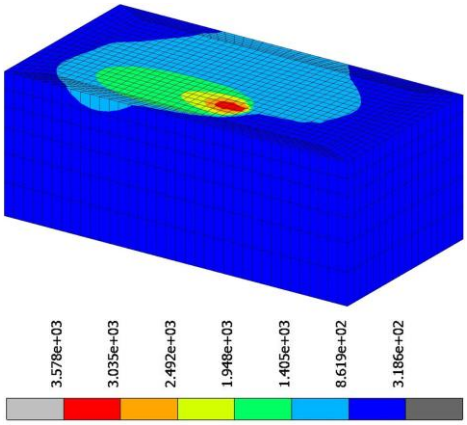

Fig. **2** First layer thermal results

3.2. Modified island scanning strategy

A mesh-based modified island scanning strategy is introduced as an alternative to the conventional rectangle-based island approach, by leveraging Rhinoceros/Grasshopper. The model and procedural steps are described in Fig. 3. Initially, the model was sliced, and the proposed strategy was implemented. Fig. Fig. 3 visually highlights the distinctions between the functional and conventional island scanning strategies. Furthermore, Table 3 provides statistical insights into the scan length for both strategies. In this context, each island on a layer is patterned with a 45° and 67° hatch angle, along with a $110\mu m$ hatch distance. The functional strategy demonstrates a more uniform distribution of scan lengths across the layer. On the other hand, the results of the short scan vector examination are shown in Table 4. The functional island strategy is beneficial for reducing short scan vectors, which can cause heat accumulation [7].

Table 3. Standard deviation

	45		67		Std. Dev. Diff	
	Mesh	Square	Mesh	Square	Mesh	Square
Std. Dev.	1.77	1.86	1.53	1.68	-7.5%	-
Mean	3.19	3.16	3.28	3.4	-	-

Table 4. Scan length examination

Strategy	Randomized		67		0	
Length	Mesh	Square	Mesh	Square	Mesh	Square
<1	2754	3600	3008	4272	1272	272
<0.5	1382	2206	1510	2723	588	163
>0.25	701	1518	768	1966	306	92
<0.1	293	1101	317	1496	104	46
>0	24117	24575	25308	26323	3008	4272

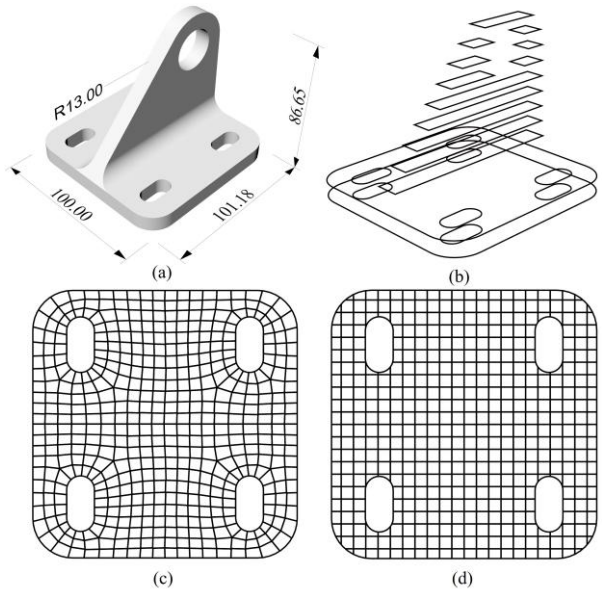

Fig. 3 (a) Model (b) Contours (c) Mesh-based modified islands (d) Conventional islands

3.3. Scan sequence determination

In this research, the challenge of determining the optimal scan sequence for the islands is addressed by conceptualizing it as a variant of the TSP, thereby leveraging the well-established strategies and algorithms associated with TSP to efficiently manage and optimize the scanning order. The establishment of an efficient scanning order is critically linked to minimizing residual stress and distortions. Additionally, the TSP framework is extended to MTSP to better represent scenarios involving multiple lasers.

Given a set of n island centers, with the distance between each pair of centers (i, j) denoted by d_{ij}, the task is to find a sequence that sorts these centers to minimize the overall path length. This is a variant of the TSP, where the cities are island centers. The mathematical formulation is as follows:

$$\min \sum_{i=1}^{n} \sum_{j=1, j\neq i}^{n} d_{ij} x_{ij} \tag{16}$$

subject to

$$\sum_{i=1, i\neq j}^{n} x_{ij} = 1 \qquad \forall j \in \{1,\ldots,n\}, \tag{17}$$

$$\sum_{j=1, j\neq i}^{n} x_{ij} = 1 \quad \forall i \in \{1,\ldots,n\}, \tag{18}$$

$$\text{where} \quad x_{ij} \in \{0,1\} \quad \forall i, j \in \{1,\ldots,n\} \tag{19}$$

with x_{ij} representing a binary variable that is 1 if the route goes directly from island center i to island center j, and 0 otherwise.

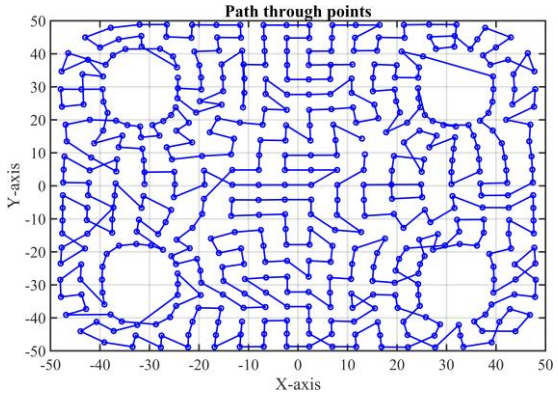

Fig. 4 One laser case

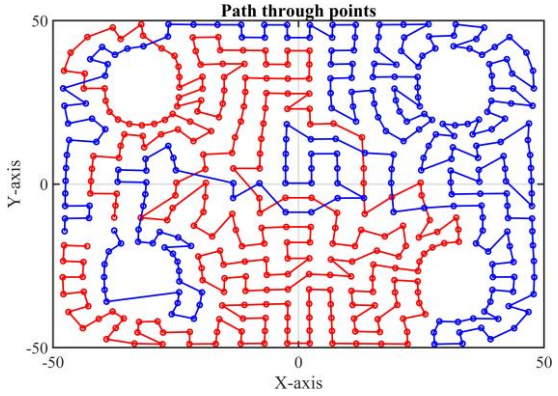

Fig. 5 Two laser case

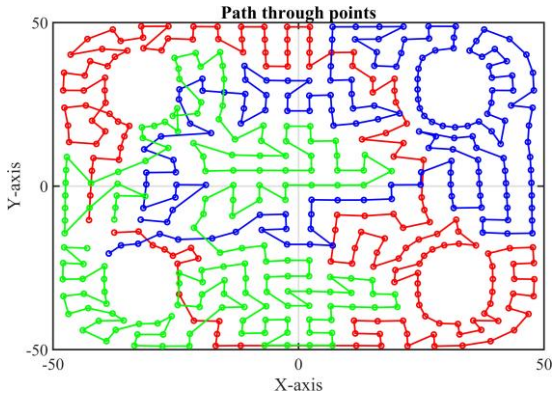

Fig. 6 Three laser case

Fig. 4, Fig. 5 and Fig. 6 illustrates the one, two and three lasers' solutions. In the next section, this approach is

applied to the part shown in Fig. 7, which is analyzed thermally.

3.4. Numerical results

Despite the practical application of TSP to real part sizes, conducting detailed transient thermal analysis at these scales is not feasible due to the high computational cost. Therefore, to maintain the complexity of the part to which TSP is applied and to demonstrate the implementation of functional islands, a part with an open hole that allows for thermal analysis was selected.

Three-dimensional transient thermal analyses were carried out on the component depicted in Fig. 7. The objective of this investigation was to comprehend the thermal behavior and dynamics of the part over time. A comparative assessment of the raster and island scanning strategies was performed, focusing on their respective thermal histories for a single layer. This comparative analysis aimed to elucidate the distinct thermal behaviors associated with each scanning strategy during the additive manufacturing process. The simulation parameters are detailed in Table 5. Simulating one layer of this component required 4982 steps for the raster strategy and 5207 steps for the island scanning strategy. A total of 143 nodes were strategically chosen, and their temperature histories were extracted. Statistical analyses, as in Fig. 8, indicate that the cooling rates for the island strategy exhibit a more uniform distribution across the entire area.

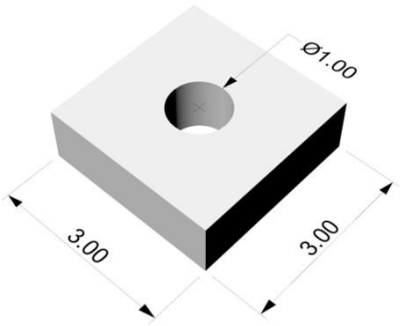

Fig. 7 Model for FEM (units are mm)

Table 5. Simulation Parameters

Simulation Parameter	Values	Nomenclature
Laser power $[\mathrm{W}]$	285	P
Scanning speed $[\mathrm{m/s}]$	0.96	v_s
Hatch spacing $[\mathrm{mm}]$	0.11	h_d
Beam radius-x $[\mathrm{m}]$	50×10^{-6}	r_x
Beam radius-y $[\mathrm{m}]$	50×10^{-6}	r_y
Beam radius-z $[\mathrm{m}]$	125×10^{-6}	r_z
Transient time $[\mathrm{s}]$	1.4×10^{-5}	Δt_{min}

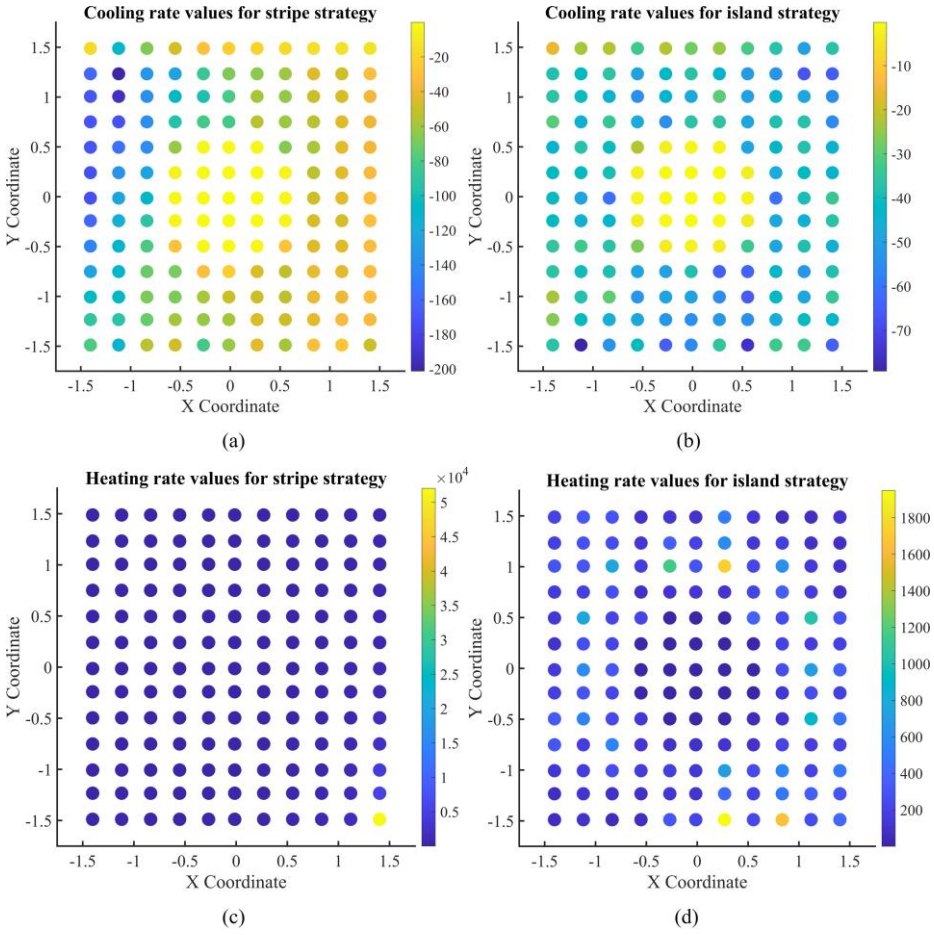

Fig. 8 (a) Cooling rate values for raster (b) Cooling rate values for island (c) Heating rate values for raster (d) Heating rate values for island

4. Conclusion

In this study, a novel mesh-based modification was introduced to the island scanning strategy, aiming to enhance the geometric integrity of manufactured components. It is demonstrated that the functional island strategy is beneficial for optimizing the scan vector lengths. Furthermore, a sophisticated scan sequencing framework was developed for both single and multi-laser configurations, employing the principles of the TSP and refining it through the application of a GA. TSP is a well-known problem, and the GA we employed for its solution is also suitable for future planned multi-objective optimization. Additionally, transient thermal analyses were conducted on both the raster and island scanning strategies. While the island scanning strategy was found to increase thermal uniformity, it is crucial to expand the exploration through more intricate and comprehensive analyses at the scale of individual components. With advancements in analysis capabilities or the application of methods such as inherent strain, part-scale thermal analyses may become feasible for functional islands as well. Equally crucial is the undertaking of experimental investigations to assess mechanical characteristics and microstructural details, which will contribute to a more profound understanding of the effects of these advanced scanning strategies.

GAs are particularly suitable for solving multi-objective problems due to their ability to handle complex and conflicting objectives. In the future, leveraging multi-objective GAs can enable optimization not only of the scanning sequence but also of other critical factors such as temperature gradients and cooling rates, leading to more comprehensive and effective solutions in metal additive manufacturing.

Acknowledgments

The financial support provided by the Scientific and Technological Research Council of Turkey (TUBITAK) under grant Numbers: 218M712, 218M713 and 218M714 are greatly acknowledged.

Author's statement

Conflict of interest: Authors state no conflict of interest.

References

[1] H. Jia, H. Sun, H. Wang, Y. Wu, and H. Wang, "Scanning strategy in selective laser melting (SLM): a review," *Int. J. Adv. Manuf. Technol.*, vol. 113, pp. 2413–2435, 2021.

[2] M. F. Zaeh and G. Branner, "Investigations on residual stresses and deformations in selective laser melting," *Prod. Eng.*, vol. 4, no. 1, pp. 35–45, Feb. 2010.

[3] R. Sebastian, S. Catchpole-Smith, M. Simonelli, A. Rushworth, H. Chen, and A. Clare, "'Unit cell'type scan strategies for powder bed fusion: The Hilbert fractal," *Addit. Manuf.*, vol. 36, p. 101588, 2020.

[4] J.-P. Kruth, J. Deckers, E. Yasa, and R. Wauthlé, "Assessing and comparing influencing factors of residual stresses in selective laser melting using a novel analysis method," *Proc. Inst. Mech. Eng. Part B J. Eng. Manuf.*, vol. 226, no. 6, pp. 980–991, 2012.

[5] M. Guo, Y. Ye, X. Jiang, and L. Wang, "Microstructure, mechanical properties and residual stress of selective laser melted AlSi10Mg," *J. Mater. Eng. Perform.*, vol. 28, pp. 6753–6760, 2019.

[6] L. Wang *et al.*, "Investigation of performance and residual stress generation of AlSi10Mg processed by selective laser melting," *Adv. Mater. Sci. Eng.*, vol. 2018, pp. 1–12, 2018.

[7] L. A. Parry, I. A. Ashcroft, and R. D. Wildman, "Geometrical effects on residual stress in selective laser melting," *Addit. Manuf.*, vol. 25, pp. 166–175, 2019.

[8] B. Cheng, S. Shrestha, and K. Chou, "Stress and deformation evaluations of scanning strategy effect in selective laser melting," *Addit. Manuf.*, vol. 12, pp. 240–251, Oct. 2016.

[9] M. Masoomi, S. M. Thompson, and N. Shamsaei, "Laser powder bed fusion of Ti-6Al-4V parts: Thermal modeling and mechanical implications," *Int. J. Mach. Tools Manuf.*, vol. 118–119, pp. 73–90, 2017.

[10] S. Zou *et al.*, "Numerical analysis of the effect of the scan strategy on the residual stress in the multi-laser selective laser melting," *Results Phys.*, vol. 16, 2020.

[11] D. Ramos, F. Belblidia, and J. Sienz, "New scanning strategy to reduce warpage in additive manufacturing," *Addit. Manuf.*, vol. 28, pp. 554–564, 2019.

[12] L. Parry, I. A. Ashcroft, and R. D. Wildman, "Understanding the effect of laser scan strategy on residual stress in selective laser melting through thermo-mechanical simulation," *Addit. Manuf.*, vol. 12, pp. 1–15, Oct. 2016.

[13] C. Bayraktar and E. Demir, "A thermomechanical finite element model and its comparison to inherent strain method for powder-bed fusion process," *Addit. Manuf.*, vol. 54, p. 102708, 2022.

[14] E. R. Denlinger, M. Gouge, J. Irwin, and P. Michaleris, "Thermomechanical model development and in situ experimental validation of the Laser Powder-Bed Fusion process," *Addit. Manuf.*, vol. 16, pp. 73–80, Aug. 2017.

[15] J. Yin *et al.*, "Dual-beam laser-matter interaction at overlap region during multi-laser powder bed fusion manufacturing," *Addit. Manuf.*, vol. 46, 2021.

[16] H. Wong, K. Dawson, G. A. Ravi, L. Howlett, R. O. Jones, and C. J. Sutcliffe, “Multi-laser powder bed fusion benchmarking—Initial trials with Inconel 625,” *Int. J. Adv. Manuf. Technol.*, vol. 105, pp. 2891–2906, 2019.

[17] J. Goldak, A. Chakravarti, and M. Bibby, “A new finite element model for welding heat sources,” *Metall. Trans. B*, vol. 15, no. 2, pp. 299–305, Jun. 1984.

[18] K. C. Mills, “Ni - IN 718,” *Recomm. Values Thermophys. Prop. Sel. Commer. Alloy.*, vol. 5, no. 4, pp. 181–190, Jan. 2002.

[19] Microsoft, “Visual Studio,” 2022. [Online]. Available: https://visualstudio.microsoft.com/

[20] M. S. C. Software, “MSC MARC,” 2023. [Online]. Available: https://www.mscsoftware.com/product/marc

[21] Q. Chen *et al.*, “An inherent strain based multiscale modeling framework for simulating part-scale residual deformation for direct metal laser sintering,” *Addit. Manuf.*, vol. 28, pp. 406–418, Aug. 2019.